

Endowing Single-Chain Polymer Nanoparticles with Enzyme-Mimetic Activity

Irma Perez-Baena,[†] Fabienne Barroso-Bujans,[†] Urs Gasser,[‡] Arantxa Arbe,[†] Angel J. Moreno,[†] Juan Colmenero,^{†,§,||} and José A. Pomposo^{*,†,§,⊥}

[†]Centro de Física de Materiales (CSIC, UPV/EHU)-Materials Physics Center, Paseo Manuel de Lardizabal 5, 20018 San Sebastián, Spain

[‡]Laboratory for Neutron Scattering, Paul Scherrer Institut, CH-5232 Villigen, Switzerland

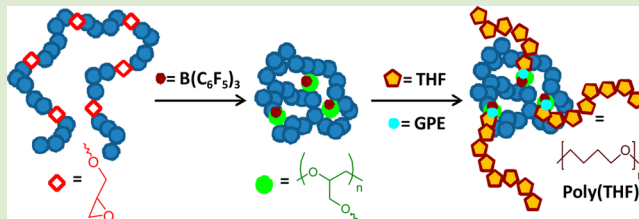
[§]Departamento de Física de Materiales, Universidad del País Vasco (UPV/EHU), Apartado 1072, 20800 San Sebastián, Spain

^{||}Donostia International Physics Center (DIPC), Paseo Manuel de Lardizabal 4, 20018 San Sebastián, Spain

[⊥]IKERBASQUE - Basque Foundation for Science, Alameda Urquijo 36, 48011 Bilbao, Spain

Supporting Information

ABSTRACT: The development of simple, efficient, and robust strategies affording the facile construction of biomimetic organocatalytic nano-objects is currently a subject of great interest. Herein, a new pathway to artificial organocatalysts based on partially collapsed individual soft nano-objects displaying useful and diverse biomimetic catalytic functions is reported. Single-chain polymer nanoparticles endowed with enzyme-mimetic activity synthesized following this new route display (i) a relatively extended morphology under good solvent conditions, as revealed by small angle neutron scattering and coarse-grained molecular dynamics simulation results, (ii) multiple, compartmentalized, and accessible catalytic sites in which borane catalytic units are retained via B··O interactions, and (iii) unprecedented reductase and polymerase enzyme-mimetic properties.



Single-chain polymer nanoparticles (SCNPs) have recently gained prominence in nanoscience and nanotechnology due to the exceptional and sometimes unique properties displayed by such nano-objects.^{1–6} SCNPs based on self-collapsed individual chains mimic the structure of folded biomacromolecules, although in a rough, primitive manner.^{7–14} Recently, we have demonstrated a very efficient strategy for the construction of transient binding disordered protein-mimic nano-objects based on SCNPs.¹⁵ Small angle neutron scattering (SANS) and molecular dynamics (MD) simulation results undoubtedly showed that the form factor of these SCNPs in solution resembles that of intrinsically disordered proteins (IDPs). Even without the precise sequence of proteins, the mimicking of IDPs morphology under good solvent conditions was a consequence of the intrachain self-assembly process leading to the formation of local globules along the individual polymer chains. In resemblance to transient binding IDPs, the resulting SCNPs were able to temporarily bind vitamin B₉ molecules that were further delivered in a controlled manner. Conversely, individual globular nano-objects were observed by transmission electron microscopy (TEM) in the dry state.

Enzyme-mimic catalytic nano-objects have been previously demonstrated based on a variety of molecular structures and nanoentities such as macrocyclic compounds,¹⁶ star¹⁷ and helical¹⁸ polymers, dendrimers¹⁹ and micelles.²⁰ However, the construction of bioinspired catalysts based on individual self-

collapsed chains is challenging due to the polydisperse nature (in size and composition) of current synthetic polymers and the lack of efficient folding protocols. Nevertheless, in a pioneering work by Wulff et al.,²¹ the synthesis of cross-linked unimolecular SCNPs containing, on average, one active site per particle was demonstrated using an “imprinted particle” method. The catalytic sites were imprinted during the synthesis of cross-linked nanogel particles via a diphenyl phosphate template that was subsequently removed from each particle. The resulting soluble nano-objects of 40 kDa in molecular weight showed Michaelis–Menten kinetics for carbonate hydrolysis, in close analogy to natural enzymes although with very low turnover frequency (TOF = $4.4 \times 10^{-3} \text{ h}^{-1}$). More recently, Terashima et al.²² have reported a synthetic route to individual amphiphilic nanoparticles that catalyze carbonyl reductions in water. After entrapment of a ruthenium (Ru)-based catalyst via ligand-exchange reaction, an amphiphilic segmented terpolymer of 105 kDa was intramolecularly self-assembled in water to give individual nanoparticles containing about 2.5 Ru atoms per particle. Quantitative reduction of cyclohexanone to cyclohexanol in 18 h was demonstrated by using only 0.5 mol % of supported Ru catalyst (TOF = 11 h^{-1}).

Received: July 18, 2013

Accepted: August 13, 2013

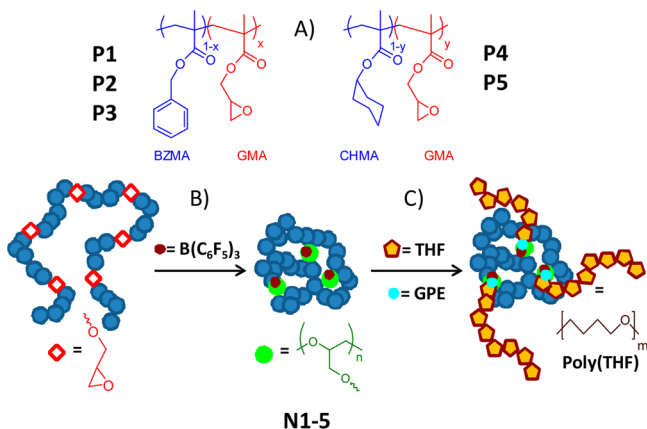
Published: August 15, 2013



This “hydrophobic cavity” approach has been further used with success by Huerta et al.²³ for performing L-proline catalyzed aldol reactions (TOF = 2 h⁻¹).

In this letter, we report a new pathway to endow SCNPs with enzyme-mimetic activity that relies on the selection of appropriate SCNP precursors allowing concurrent catalyst-assisted intrachain cross-linking and binding of the catalyst to intramolecular SCNP sites. As a proof of the concept, SCNPs were synthesized from glycidyl precursors under B(C₆F₅)₃-catalyzed intramolecular cross-linking. While the driving force for SCNP formation was B(C₆F₅)₃-assisted intrachain ring-opening polymerization (ROP) of glycidyl moieties, the simultaneous binding of B(C₆F₅)₃ units to oxygen-containing functional groups (ether, carbonyl) of the cross-linked GMA moieties via B⋯O interactions endowed the resulting SCNPs with reductase and polymerase enzyme-mimetic activity (see Scheme 1). In contrast with enzymes where the driving force

Scheme 1. (A) Chemical Structure of Precursors P1–5 (BZMA = Benzyl Methacrylate; CHMA = Cyclohexyl Methacrylate; GMA = Glycidyl Methacrylate); (B) Synthesis of SCNPs N1–5 Endowed with Enzyme-Mimetic Activity from Glycidyl Precursors P1–5 through Concurrent B(C₆F₅)₃-Assisted Intrachain Ring-Opening Polymerization and Binding of B(C₆F₅)₃ Catalyst Molecules via B⋯O Interactions; (C) Synthesis of Poly(tetrahydrofuran), Poly(THF), in the Presence of Catalytic Amounts of Glycidyl Phenyl Ether (GPE) Using the Polymerase-Like Properties of the Organocatalytic SCNPs N1–5



for folding depends on the sequence of amino acids, their mutual interactions and their interactions with solvent molecules, precursor self-assembly to SCNPs was driven by B(C₆F₅)₃-catalyzed ROP of intrachain glycidyl groups. Enzyme-mimetic catalytic activity resulted from B(C₆F₅)₃-immobilization in multiple, compartmentalized internal nanoparticle sites that were accessible to reagents. Tuning of SCNP size, which presumably influences the size, composition, number, and placement of catalytic compartments, was found to have a significant effect on kinetics and, consequently, on turnover frequency during organocatalysis (vide infra).

Because SCNP size at constant glycidyl content was expected to depend on polymeric precursor molecular weight,^{7,24} different SCNP precursors (P1–5) having weight average molecular weight (M_w) above 1000 kDa or below 100 kDa were synthesized by random copolymerization of glycidyl methacrylate (GMA) with benzyl methacrylate (BZMA) or cyclohexyl methacrylate (CHMA). We selected BZMA and

CHMA to increase the guest coordination of B(C₆F₅)₃ moieties to cross-linked glycidyl groups from GMA moieties.²⁵ To minimize intermolecular coupling events while allowing significant intrachain collapse, target GMA content in the precursors was selected to be around 30 mol %.^{7,11} SCNP precursors showing $M_w < 100$ kDa and narrow molecular weight distribution ($M_w/M_n < 1.1$) were synthesized in high yield (>80%) by reversible addition–fragmentation chain transfer (RAFT) polymerization. SCNP precursors showing $M_w > 1000$ kDa while retaining moderate polydispersity values ($M_w/M_n < 1.6$) were obtained by free radical polymerization under controlled synthesis conditions, at fractional conversion $c < 0.2$. The main characteristics of SCNP precursors P1–5 synthesized in this work are reported in Table 1.

Table 1. Characteristics of the Precursors P1–5

precursor #	GMA ^a (mol %)	M_w ^b (kDa)	M_w/M_n ^c	R_h ^d (nm)
P1	35	1912	1.39	20
P2	31	2330	1.68	23
P3	31	48.1	1.05	3
P4	27	2641	1.55	25
P5	30	46.0	1.06	3

^aContent of GMA in the precursor as determined by ¹H NMR spectroscopy. ^bActual molecular weight as determined by combined SEC/MALS measurements. ^c M_w = weight average molecular weight. M_n = number average molecular weight. ^dHydrodynamic radius, R_h , as determined by DLS measurements.

SCNP synthesis was performed in methylene chloride at room temperature under diluted conditions (0.3 mg/mL for SCNP precursors showing $M_w > 1000$ kDa and 1 mg/mL otherwise) to guarantee individual soft nanoparticle formation through B(C₆F₅)₃-assisted intrachain ROP of the glycidyl moieties. SCNP synthesis at higher concentration would be performed with the assistance of a continuous addition technique.^{7,8} The irreversible collapse accompanying organocatalytic SCNP formation was clearly identified by size exclusion chromatography (SEC) due to the increase in retention time shown by the internally cross-linked SCNPs. As an example, Figure 1A shows the SEC chromatograms of precursor P1 and the resulting SCNPs, denoted as N1, after 24 h of reaction time. It is worth mentioning that the retention time in SEC measurements is inversely proportional to the hydrodynamic size, so a longer SCNP vs precursor SEC retention time (i.e., a lower value of “apparent” M_w) is indicative of a more crumpled structure.²⁶ Actual M_w values for SCNPs N1–5, as determined from static light scattering (SLS) data, were consistent to those of the corresponding P1–5 precursors (see Table 2).^{27,28}

Complementary dynamic light scattering (DLS), transmission electron microscopy (TEM), and atomic force microscopy (AFM) measurements provided evidence of individual SCNP formation. A reasonable agreement was found between data from different techniques (probably due to the presence of residual solvent in the samples during TEM and AFM measurements). As a representative example, the average diameter of N1 from AFM (gold substrate, Figure 1B), DLS (chloroform solution, Figure S1), and TEM (carbon-coated grid, Figure S2) measurements was found to be 36, 35, and 40 nm, respectively. Upon intrachain ROP of the GMA units,^{29–33} a complete disappearance of the ¹H NMR bands corresponding to glycidyl protons was observed (Figure 1C).

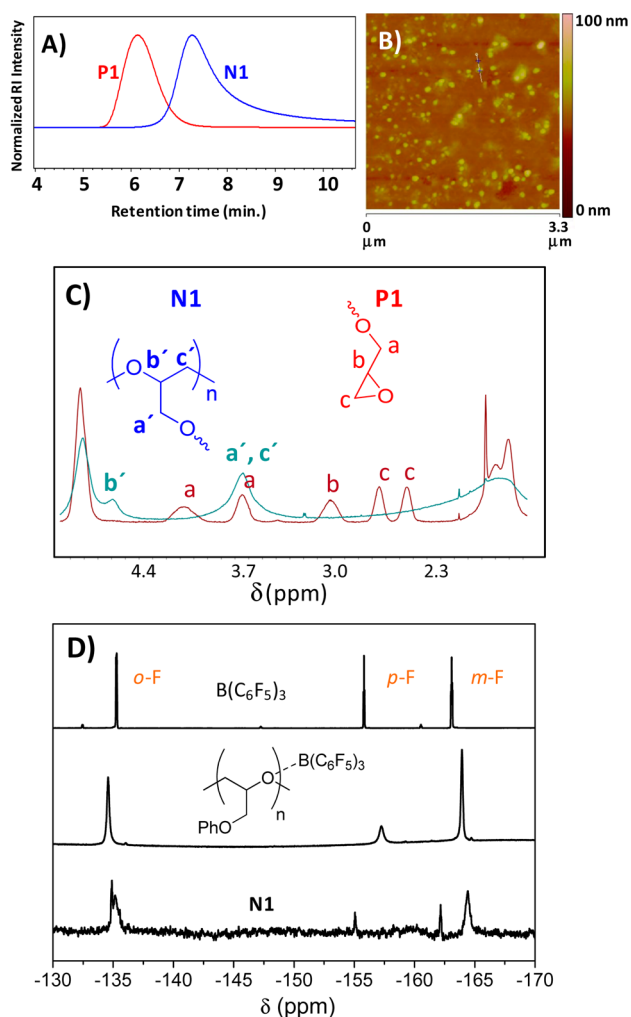


Figure 1. (A) SEC chromatograms of the SCNP precursor P1 and the resulting organocatalytic SCNP N1. (B) AFM picture of SCNP N1 (dry state) showing an average nanoparticle size of 36 nm (height size). (C) ^1H NMR spectra of precursor P1 and SCNP N1 in the region of the glycidic proton bands. (D) ^{19}F NMR spectra of $\text{B}(\text{C}_6\text{F}_5)_3$ (top), poly(GPE) synthesized via $\text{B}(\text{C}_6\text{F}_5)_3$ -catalyzed ROP (middle) and SCNP N1 (bottom).

Table 2. Characteristics of SCNPs N1–5 Synthesized from Precursors P1–5

SCNP #	$\text{B}(\text{C}_6\text{F}_5)_3$ content ^a	M_w , app ^b (kDa)	M_w , c (kDa)	M_w/M_n ^d	R_h ^e (nm)
N1	4.4	610	2010	1.20	17
N2	4.2	690	2450	1.33	19
N3	5.1	37.2	49.1	1.05	2
N4	4.5	1304	2614	1.41	20
N5	4.9	35.1	46.9	1.05	1.5

^a $\text{B}(\text{C}_6\text{F}_5)_3$ content (wt %) in the SCNPs as determined by TGA measurements. ^bApparent molecular weight as determined by conventional SEC measurements. ^cActual molecular weight as determined by combined SEC/MALS measurements. ^d M_w = weight average molecular weight. M_n = number average molecular weight. ^eHydrodynamic radius, R_h , as determined by DLS measurements.

SCNP formation was found to complete after only 3 h of reaction time, pointing to a very fast intrachain ROP process (Figure S3). We have estimated from thermal gravimetric analysis (TGA) data that on average a single N1 macro-

molecule contains around 165 borane units, that is, one $\text{B}(\text{C}_6\text{F}_5)_3$ molecule every 25 GMA moieties or, alternatively, one $\text{B}(\text{C}_6\text{F}_5)_3$ unit every 70 (GMA + BZMA) repeat units corresponding to a local environment of about 11.6 kDa in molecular weight (Figure S4). Consequently, each SCNP exhibits a relatively large amount of compartmentalized, internal active catalytic sites. Figure 1D provides a comparison of the ^{19}F NMR spectra of $\text{B}(\text{C}_6\text{F}_5)_3$, poly(glycidyl phenyl ether)-poly(GPE)- synthesized via $\text{B}(\text{C}_6\text{F}_5)_3$ -catalyzed ROP, and SCNP N1. As expected, $\text{B}(\text{C}_6\text{F}_5)_3$ shows well-defined signals that can be assigned to *o*-F, *m*-F, and *p*-F atoms from C_6F_5 rings. Similarly, poly(GPE) containing residual $\text{B}(\text{C}_6\text{F}_5)_3$ molecules shows slightly broader, but clear *o*-F, *m*-F, and *p*-F peaks. On the other hand, due to the efficient binding of $\text{B}(\text{C}_6\text{F}_5)_3$ moieties within the SCNP during the folding/collapse process via $\text{B}\cdots\text{O}$ interactions, only relatively broad, low-intensity bands are seen in Figure 1D, arising presumably from F atoms in $\text{B}(\text{C}_6\text{F}_5)_3$ units located at the most external part of the nanoparticles. In this sense, it is worth noting that F atoms placed in a relatively solid-like environment are expected to be nondetectable by liquid-state ^{19}F NMR spectroscopy giving rise to a reduction in signal intensity as observed in Figure 1D for SCNP N1. X-ray photoelectron spectroscopy (XPS) measurements were in good agreement with TGA and ^{19}F NMR results. However, attempts to characterize the chemical state of the immobilized boron atoms in SCNPs N1–5 by XPS failed due to the small amount of boron atoms at the nanoparticle surface (Figure S5).

Additional small angle neutron scattering (SANS) experiments in deuterated solvent, which did not show the presence of multichain aggregates, confirmed the unimolecular nature of the organocatalytic nanoparticles (Figure 2A). Complementary

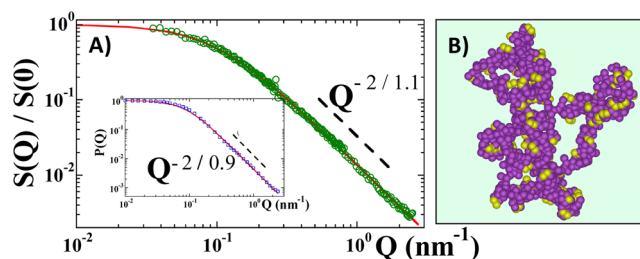


Figure 2. (A) SANS results revealing the form factor of SCNP N1 in solution (green circles) and calculated form factor from MD simulations (inset, blue squares). Solid lines are Ornstein–Zernike fits.³⁴ Dashed lines represent the asymptotic regime $S(Q) \sim Q^{-2/\nu}$. (B) Typical snapshot from MD simulations showing the relatively open structure of an organocatalytic SCNP under good solvent conditions.

molecular dynamics (MD) simulations of the folding/collapse process during nanoparticle formation under good solvent conditions suggested that the resulting SCNPs N1–5 show a relatively open/extended morphology in solution, which is a very convenient feature for catalysis applications (see SI for SANS and MD simulation details and Figure S6 and S7). For SCNP N1, a comparison of results from SANS measurements and MD simulations is provided in Figure 2A. The SCNP form factor was fitted using conventional Ornstein–Zernike formalism.³⁴ SANS measurements and MD simulations deliver practically the same value of the scaling exponent ($\nu = 1.1$ and 0.9, respectively), much closer to that characterizing a Gaussian chain ($\nu = 1$) than to that expected for spherical objects ($\nu \approx 1/2$). The excellent agreement between

experiment and MD simulations validates the typical nanoparticle morphology in good solvent (snapshot from MD simulations) illustrated in Figure 2B. Gaussian chain-like behavior of single-chain nanoparticles in solvents of good quality for the polymer precursors has been previously determined for nanoparticles of different chemical structures.²⁶ In addition, the presence of an extended-to-compact transition upon solvent removal has been recently reported for transient vitamin-binding disordered protein mimic nano-objects based on SCNPs.¹⁵

After precipitation in hexane and further drying under vacuum, the isolated SCNPs N1–5 were found to display reductase and polymerase enzyme-mimetic activity for reactions carried out in inert solvents, such as dried halogenated solvents, benzene or toluene. However, the catalytic activity was lost for reactions performed in solvents that form adducts with $B(C_6F_5)_3$ such as acetonitrile, DMSO, DMF, or alcohols, imposing limitations for the reuse of these enzyme-mimetic nano-objects (see SI). It is worth mentioning that the organocatalytic SCNP activity shown in inert solvents results from the interaction of individual $B(C_6F_5)_3$ moieties with oxygen-containing functional groups (ether, carbonyl) of the SCNPs.

To evaluate the reductase-like properties of the SCNPs, we explored the use of the enzyme-mimetic SCNPs N1–5 in the reduction of α -diketones to silyl-protected 1,2-diols as a representative model reaction.³⁵ In particular, the bis-(hydrosilylation) of benzil (2) with dimethylphenylsilane (1) in dichloromethane was investigated as a function of nanoparticle loading and the results were compared to the reported, control reaction using 4 mol % of $B(C_6F_5)_3$. As summarized in Table 3, reactions carried out with only 0.3 mol % of entrapped

Table 3. Reductase-Like Properties of SCNPs N1–5 Allowing the Highly-Efficient Reduction of α -Diketones to Silyl-Protected 1,2-Diols

SCNP #	$B(C_6F_5)_3$ ^a (mol %)	reaction time (min)	yield ^b (3; %)	meso/dl ^b (%)	TOF (h ⁻¹)
	4 ^c	1	>99	79/21	1485
N1	0.3 ^d	10	>99	80/20	1980
N1	0.18 ^d	12	97	80/20	2695
N1	0.12 ^d	15	95	79/21	3170
N1	0.06 ^d				
N2	0.11 ^d	16	94	81/19	3204
N2	0.055 ^d				
N3	0.14 ^d	7	96	79/21	5880
N3	0.07 ^d				
N4	0.12 ^d	14	93	80/20	3320
N5	0.13 ^d	8	97	79/21	5595

^aWith respect to dimethylphenylsilane. ^bAs determined by ¹H NMR spectroscopy. ^cData from ref 35. ^dEntrapped in the SCNP (TOF = turnover frequency; see ref 36).

$B(C_6F_5)_3$ with respect to the amount of silane reagent gave quantitative yield of product (3), as well as a meso/dl ratio = 80/20. Very good yield was maintained by reducing the amount of catalyst up to a limiting value of 0.12 mol %, while retaining the diastereoselectivity (Table 3, Figure S8). By using SCNPs of $M_w > 1000$ kDa, the dark yellow reaction medium turned to colorless typically in less than 15 min when compared to about 1 min for the control reaction.³⁵ We attribute the longer reaction time in the former case to a slower diffusion of the

reagents to the SCNP active catalytic sites. In fact, for SCNPs of $M_w < 100$ kDa the reaction showed a typical 2-fold decrease in reaction time. The turnover frequency (TOF) defined as the number of moles of substrate that a mole of catalyst can convert per unit time³⁶ was found to be as high as about 3200 h⁻¹ for SCNPs of $M_w > 1000$ kDa (N1, N2, and N4, see Table 3). Interestingly, SCNPs of $M_w < 100$ kDa (N3 and N5) having the smallest sizes ($R_h = 1.5$ –2 nm) showed the maximum TOF values, TOF = 5880 h⁻¹ (Table 3).

Additionally, we investigated the polymerase-like activity of enzyme-mimetic SCNPs N1–5. We use the term “polymerase-like” to refer to the capacity of SCNPs N1–5 for polymerizing THF at rt in the presence of small amounts of glycidyl phenyl ether (GPE) to avoid confusion with the exquisite activity of natural polymerase enzymes that use templates (mRNA, DNA) to synthesize perfectly defined (in length and sequence) biomacromolecules.³⁷ In the case of the enzyme-mimetic organocatalytic SCNPs N1–5, we found that GPE takes the role of cocatalyst since no poly(THF) was formed if GPE was absent (see Table S1). In this sense, the beneficial effect of some epoxides for initiating the cationic ROP of THF has been previously recognized.³⁸ We hypothesize that GPE species presumably participates in the initial reaction steps allowing stabilization of short cationic growing chains that further propagate through ROP of THF units. By working at low SCNP concentration (0.3–2 mg/mL) and low to moderate reaction time (6–48 h), poly(GPE-co-THF) copolymers of M_w in the range of 55 to 150 kDa (SEC with PS standards) with M_w/M_n values around 2.2 to 3.2 and high content of THF-based moieties were obtained (see Table S1). Increasing the SCNP concentration leads to a higher amount of soluble copolymers showing $M_w = 135$ kDa and $M_w/M_n = 1.8$ but accompanied by the generation of a certain fraction of organogel. Characterization of the soluble poly(GPE-co-THF) fraction by ¹H NMR spectroscopy revealed a content of GPE units of only 1.6 mol %, incorporated presumably at the early beginning of the ROP process (see Figure S9). In absence of THF, SCNPs N1–5 allow the ROP of GPE leading to poly(GPE) of low molecular weight ($M_w = 6.5$ kDa and $M_w/M_n = 2.2$). In this case, organogel formation was not observed even by working at high loading of SCNPs N1–5 and up to high conversion. Several factors could contribute to organogel formation. First, the presumably depletion interactions between particles caused by the presence of high molecular weight polymers in the reaction medium could lead to significant interparticle attraction at high SCNP concentration.³⁹ Hence, the probability of a growing poly(GPE-co-THF) chain initiated in a given SCNP to connect with another SCNP will increase. Second, the probability of transfer events stopping chain growing will certainly increase with increasing SCNP concentration. Work is in progress to elucidate the mechanism behind (and the scope of) the polymerase-like activity of enzyme-mimetic SCNPs N1–5.

In summary, a new pathway to single-chain polymer nanoparticles endowed with enzyme-mimetic activity has been introduced based on concurrent catalyst-assisted intramolecular cross-linking of linear precursors and binding of the catalyst to SCNP intrachain cross-linked sites. As a proof of the concept, organocatalytic SCNPs were synthesized from appropriate glycidyl precursors through $B(C_6F_5)_3$ -assisted intrachain ring-opening polymerization and $B(C_6F_5)_3$ binding to oxygen-containing functional groups (ether, carbonyl) of the SCNPs via B...O interactions. The resulting SCNPs, showing

multiple, compartmentalized local catalytic sites and a relatively open/extended morphology under good solvent conditions, display reductase and polymerase-like properties. This new “concurrent” strategy for endowing SCNPs with enzyme-mimetic activity broadens the previous “imprinted particle”²¹ and “hydrophobic cavity”^{22,23} routes. In the near future, new folding/collapsing activators playing simultaneously the dual role of intrachain cross-linkers and chemoselective catalysts will be explored.

■ ASSOCIATED CONTENT

Supporting Information

Materials and methods, characterization techniques, molecular dynamics (MD) simulations, and supporting data. This material is available free of charge via the Internet at <http://pubs.acs.org>.

■ AUTHOR INFORMATION

Corresponding Author

*E-mail: josetxo.pomposo@ehu.es.

Notes

The authors declare no competing financial interest.

■ ACKNOWLEDGMENTS

Financial support from the Projects MAT2012-31088 (MINECO) and IT-654-13 (GV) is acknowledged. I. P.-B. acknowledges CSIC for her JAE-PREDOC grant. We gratefully thank Musthafa Kummali, Mariano Barrado (SGIker), and David Pickup for AFM, TEM, and XPS measurements, respectively. This work is based on experiments performed at the Swiss spallation neutron source SINQ, Paul Scherrer Institute, Villigen, Switzerland, and has been supported by the European Commission under the 7th Framework Programme through the “Research Infrastructures” action of the “Capacities” Programme, NMI3-II Grant Number 283883.

■ REFERENCES

- (1) Mackay, M. E.; Dao, T. T.; Tuteja, A.; Ho, D. L.; Horn, B. V.; Kim, H.-C.; Hawker, C. J. *Nat. Mater.* **2003**, *2*, 762–766.
- (2) Hamilton, S. K.; Harth, E. *ACS Nano* **2009**, *3*, 402–410.
- (3) Oria, L.; Aguado, R.; Pomposo, J. A.; Colmenero, J. *Adv. Mater.* **2010**, *22*, 3038–3041.
- (4) Pomposo, J. A.; Ruiz de Luzuriaga, A.; García, I.; Etxeberria, A.; Colmenero, J. *Macromol. Rapid Commun.* **2011**, *32*, 573–578.
- (5) Whitaker, D. E.; Mahon, C. S.; Fulton, D. A. *Angew. Chem., Int. Ed.* **2013**, *52*, 956–959.
- (6) Zhu, B.; Sun, S.; Wang, Y.; Deng, S.; Qian, G.; Wang, M.; Hu, A. *J. Mater. Chem. C* **2013**, *1*, 580–586.
- (7) Harth, E.; Horn, B. V.; Lee, V. Y.; Germack, D. S.; Gonzales, C. P.; Miller, R. D.; Hawker, C. J. *J. Am. Chem. Soc.* **2002**, *124*, 8653–8660.
- (8) Ruiz de Luzuriaga, A.; Ormategui, N.; Grande, H. J.; Odriozola, I.; Pomposo, J. A.; Loinaz, I. *Macromol. Rapid Commun.* **2008**, *29*, 1156–1160.
- (9) Berda, E. B.; Foster, E. J.; Meijer, E. W. *Macromolecules* **2010**, *43*, 1430–1437.
- (10) Murray, B. S.; Fulton, D. A. *Macromolecules* **2011**, *44*, 7242–7252.
- (11) Appel, E. A.; del Barrio, J.; Dyson, J.; Isaacs, L.; Scherman, O. A. *Chem. Sci.* **2012**, *3*, 2278–2281.
- (12) Altintas, O.; Barner-Kowollik, C. *Macromol. Rapid Commun.* **2012**, *33*, 958–971.
- (13) Sanchez-Sanchez, A.; Perez-Baena, I.; Pomposo, J. A. *Molecules* **2013**, *3*, 3339–3355.
- (14) Gillissen, M. A. J.; Terashima, T.; Meijer, E. W.; Palmans, A. R. A.; Voets, I. K. *Macromolecules* **2013**, *46*, 4120–4125.
- (15) Sanchez-Sanchez, A.; Akbari, S.; Etxeberria, A.; Arbe, A.; Gasser, U.; Moreno, A. J.; Colmenero, J.; Pomposo, J. A. *ACS Macro Lett.* **2013**, *2*, 491–495.
- (16) Breslow, R.; Dong, S. D. *Chem. Rev.* **1998**, *98*, 1997–2011.
- (17) Inoue, K. *Prog. Polym. Sci.* **2000**, *25*, 453–571.
- (18) Yamamoto, T.; Yamada, T.; Nagata, Y.; Sugimoto, M. *J. Am. Chem. Soc.* **2010**, *132*, 7899–7901.
- (19) Liang, C.; Fréchet, J. M. J. *Prog. Polym. Sci.* **2005**, *30*, 385–402.
- (20) Wang, Y.; Xu, H.; Ma, N.; Wang, Z.; Zhang, X.; Liu, J.; Shen, J. *Langmuir* **2006**, *22*, 5552–5555.
- (21) Wulff, G.; Chong, B.-O.; Kolb, U. *Angew. Chem., Int. Ed.* **2006**, *45*, 2955–2958.
- (22) Terashima, T.; Mes, T.; De Greef, T. F. A.; Gillissen, M. A. J.; Besenius, P.; Palmans, A. R. A.; Meijer, E. W. *J. Am. Chem. Soc.* **2011**, *133*, 4742–4745.
- (23) Huerta, E.; Stals, P. J. M.; Meijer, E. W.; Palmans, A. R. A. *Angew. Chem., Int. Ed.* **2013**, *52*, 2906–2910.
- (24) Foster, E. J.; Berda, E. B.; Meijer, E. W. *J. Polym. Sci., Polym. Chem.* **2011**, *49*, 118–126.
- (25) Focante, F.; Mercandelli, P.; Sironi, A.; Resconi, L. *Coord. Chem. Rev.* **2006**, *250*, 170.
- (26) Pomposo, J. A.; Perez-Baena, I.; Buruaga, L.; Alegría, A.; Moreno, A. J.; Colmenero, J. *Macromolecules* **2011**, *44*, 8644–8649.
- (27) Tuten, B. T.; Chao, D.; Lyon, C. K.; Berda, E. B. *Polym. Chem.* **2012**, *3*, 3068–3071.
- (28) Chao, D.; Jia, X.; Tuten, B.; Wang, C.; Berda, E. B. *Chem. Commun.* **2013**, *49*, 4178–4180.
- (29) Price, C. C.; Carmelite, D. D. *J. Am. Chem. Soc.* **1966**, *88*, 4039–4044.
- (30) Hino, T.; Endo, T. *J. Polym. Sci., Polym. Chem.* **2004**, *42*, 5407–5412.
- (31) Schlaad, H.; Kukula, H.; Rudloff, J.; Below, I. *Macromolecules* **2001**, *34*, 4302–4304.
- (32) Morinaga, H.; Ochiai, B.; Endo, T. *Macromolecules* **2007**, *40*, 6014–6016.
- (33) Morinaga, H.; Ujihara, Y.; Yamanaka, T.; Nagai, D.; Endo, T. *J. Polym. Sci., Polym. Chem.* **2011**, *49*, 4092–4097.
- (34) Rubinstein, M.; Colby, R. H. *Polymer Physics*; Oxford University Press: New York, 2003.
- (35) Skjel, M. K.; Houghton, A. Y.; Kirby, A. E.; Harrison, D. J.; McDonald, R.; Rosenberg, L. *Org. Lett.* **2010**, *12*, 376–379.
- (36) Kozuch, S.; Martin, J. M. L. *ACS Catal.* **2012**, *2*, 2787–2794.
- (37) Berg, J. M.; Tymoczko, J. L.; Stryer, L. *Biochemistry*; W. H. Freeman Publishers: New York, 2002.
- (38) Hammond, J. M.; Hooper, J. F.; Robertson, W. G. P. *J. Polym. Sci., Part A-1: Polym. Chem.* **1971**, *9*, 265–279.
- (39) Asakura, S.; Oosawa, F. *J. Polym. Sci.* **1958**, *33*, 183–192.